Mechanical Consequences of Cell-Wall Turnover in the Elongation of a Gram-Positive Bacterium

Gaurav Misra,[†] Enrique R. Rojas,[†] Ajay Gopinathan,[‡] and Kerwyn Casey Huang[†*]
[†]Department of Bioengineering, Stanford University, Stanford, California; and [‡]Department of Physics, University of California, Merced, California

ABSTRACT A common feature of walled organisms is their exposure to osmotic forces that challenge the mechanical integrity of cells while driving elongation. Most bacteria rely on their cell wall to bear osmotic stress and determine cell shape. Wall thickness can vary greatly among species, with Gram-positive bacteria having a thicker wall than Gram-negative bacteria. How wall dimensions and mechanical properties are regulated and how they affect growth have not yet been elucidated. To investigate the regulation of wall thickness in the rod-shaped Gram-positive bacterium *Bacillus subtilis*, we analyzed exponentially growing cells in different media. Using transmission electron and epifluorescence microscopy, we found that wall thickness and strain were maintained even between media that yielded a threefold change in growth rate. To probe mechanisms of elongation, we developed a biophysical model of the Gram-positive wall that balances the mechanical effects of synthesis of new material and removal of old material through hydrolysis. Our results suggest that cells can vary their growth rate without changing wall thickness or strain by maintaining a constant ratio of synthesis and hydrolysis rates. Our model also indicates that steady growth requires wall turnover on the same timescale as elongation, which can be driven primarily by hydrolysis rather than insertion. This perspective of *turnover*-driven elongation provides mechanistic insight into previous experiments involving mutants whose growth rate was accelerated by the addition of lysozyme or autolysin. Our approach provides a general framework for deconstructing shape maintenance in cells with thick walls by integrating wall mechanics with the kinetics and regulation of synthesis and turnover.

INTRODUCTION

Within all kingdoms of life, cellular cytoplasm is often significantly more concentrated with solutes than the extracellular environment, producing an osmotic pressure known as turgor pressure. In many cells, turgor pressure can be several atmospheres (1). Such pressure cannot be borne by the membrane alone, and hence these cells require a stiff cell wall such as those found in plants, fungi, and bacteria. Recent studies have revealed the mechanical role of the cell wall in regulating the growth and form of eukaryotes, controlling tip growth in *Schizosaccharyomyces pombe* (fission yeast) (2) and pollen tubes (3), and guiding *Lilium longiflorum* (Easter lily) pollen grains toward distinct desiccation-prevention folding pathways and assisting pollen closure (4). In virtually all bacteria, the cell wall is necessary and sufficient for cell-shape determination (5), and is constantly remodeled during growth (6). The major constituent of the bacterial cell wall is peptidoglycan, a macromolecule that is built from disaccharide chains (glycans) cross-linked by short peptides (6). Although the biochemical composition and assembly pathway of the cell-wall network are well known, it is largely unknown how its dimensions are established and maintained during growth. In particular, the thickness of the wall across bacterial species is highly variable, ranging from the monolayer-thick walls of Gram-negative species such as *Escherichia coli* to the ~100-nm-thick walls of Gram-positive species such as *Corynebacterium glutamicum*.

The high solute and nutrient concentrations in the cytoplasm of Gram-positive bacteria lead to a relatively high internal osmotic pressure, which can be up to 30 atm (1,7). How bacteria grow and divide in the presence of a high turgor pressure has motivated theoretical (8–13) and experimental studies (14–18) of the structure and mechanical properties of the cell envelope. According to the inside-to-outside growth hypothesis proposed by Koch (19) and Koch and Doyle (20), unstressed peptidoglycan is laid down in layers on the inner side of the wall while the outer (older) layers are degraded by autolysis. As the outermost layer is sloughed off into the medium, all remaining layers stretch to bear the longitudinal stress due to turgor pressure. Although this model suggests a biophysical basis for the elongation of Gram-positive bacteria, it remains untested because experimental predictions of such a model have not been described.

Bacillus subtilis is a model rod-shaped, Gram-positive bacterium that has been used in extensive studies of wall biochemistry and structure. Cryo-electron microscopy (cryo-EM) of *B. subtilis* grown in Lennox broth (LB), a nutrient-rich medium, indicates that the cell-wall thickness is relatively constant across cells (21). Moreover, regulated degradation of the wall is necessary for normal growth (22), suggesting that wall turnover and synthesis are coupled in some fashion (23,24). Under conditions of nutrient deprivation or harsh environmental conditions, *B. subtilis* cells can

Submitted October 10, 2012, and accepted for publication April 5, 2013.
*Correspondence: kchuang@stanford.edu
Editor: David Odde.

0006-3495/13/06/2342/11 $2.00
http://dx.doi.org/10.1016/j.bpj.2013.04.047

survive through a process known as sporulation, in which they divide asymmetrically to produce a forespore. The engulfment stage of sporulation, in which a membrane and cell wall are synthesized to surround the forespore within the mother cell cytoplasm, involves a choreographed spatiotemporal pattern of membrane synthesis, and both cell-wall synthesis and degradation. Directly before the onset of engulfment, hydrolase-mediated degradation of the peptidoglycan between the septal membranes is necessary to allow the mother cell membrane to migrate around the forespore (25,26), and wall synthesis and hydrolysis are colocalized at the leading edge of the engulfing membrane (27,28). Thus, the wall properties and biochemical regulation in different growth conditions provide a strong constraint for biophysical models of turgor-mediated wall growth (29).

In this work, we experimentally characterized the growth rate, wall thickness, and mechanical strain (extension relative to an unstressed state) of *B. subtilis* cells grown in a rich medium (LB) and a minimal medium (MM). Although the growth rate was threefold smaller in MM than in LB, the average wall thickness and strain were essentially unchanged. To understand the molecular mechanism underlying these observations, we developed a mechanochemical model for the elongation of a rod-shaped Gram-positive bacterium, conceptualizing its cell wall as an elastic, layered network. In this model, the turgor pressure is the primary driving force for elongation, and we used simulations to explore the effects of the rates of wall synthesis and enzymatic hydrolysis on growth rate, wall thickness, and strain. Our model suggests that a cell in which the rate of cell-wall synthesis is proportional to the rate of hydrolysis can vary its growth rate independently of wall thickness and global strain. Moreover, our results indicate that fast growth in rich medium requires high rates of turnover of cell-wall material, and suggest a counterintuitive acceleration of growth of Gram-positive bacteria when treated with antibiotics that inhibit cell-wall synthesis or under conditions in which densely packed cells can share enzymes responsible for turnover.

MATERIALS AND METHODS

Bacterial growth and imaging conditions

Because *B. subtilis* cells could not be propagated solely in M9+0.4% glucose, we define an MM culture as a 1:100 dilution of LB stationary phase culture in M9+0.4% glucose. For imaging experiments, individual liquid cultures of *B. subtilis* strains 168, FC332, and AH93 were prepared by diluting overnight cultures 1:100 into fresh media. In contrast to *B. subtilis* 168, strain FC332 is nonchaining and hence isolated cells could be readily identified. Media for AH93 cultures also contained 20 mM xylose and 4 μg/mL chloramphenicol. Cultures were grown at 37°C with shaking into exponential phase with an optical density of 0.3–0.5 at 600 nm in LB or 0.05–0.08 in MM. The bulk growth rates of liquid cultures were measured with a Tecan Infinite 200 PRO plater reader (Tecan Group Ltd., San Jose, CA). For live-cell imaging, we pipetted exponentially growing cells onto a 1% agarose pad containing the appropriate medium. All phase-contrast and fluorescence micrographs were captured with a Nikon Ti-E microscope (Nikon, Tokyo, Japan) and a DU-885 cooled CCD camera (Andor Technology, Belfast, Ireland) using μManager 1.3 software. Cell shape was analyzed using the MATLAB (The MathWorks, Natick, MA) software MicrobeTracker (30).

Single-cell growth-rate measurements

B. subtilis 168 cells were grown in ONIX Microfluidic Plates (CellASIC, Hayward, CA) for 60 min in LB or 120 min in MM and imaged every 2 min. Images were analyzed using MicrobeTracker to extract steady-state elongation rates. The relative growth of the cell ends was determined from the cell lengths l_1 and l_2 at successive time points t_1 and t_2 using

$$\frac{v}{l} = \frac{(l_2 - l_1)/(t_2 - t_1)}{(l_1 + l_2)/2}. \quad (1)$$

Once a cell reached a steady-state value of v/l, several subsequent measurements were averaged to obtain the relative growth rate for that cell.

Global strain measurements

B. subtilis 168 cells were grown in ONIX Microfluidic Plates in either LB or MM for 30 min to ensure exponential growth. The cell wall was labeled with Alexa Fluor 488 dye bound to the lectin wheat germ agglutinin (WGA; Life Technologies, Grand Island, NY) by flowing in media containing the lectin for ~5 min. The cells were then osmotically shocked with 4 M NaCl solution in appropriate media to release the turgor pressure on the wall; the cells were simultaneously imaged every 5 s in phase and fluorescence. The cell lengths before and after shock were measured using MicrobeTracker (30). The septa in chains of cells had higher WGA fluorescence than the sidewalls and hence could be used as fiducial markers. The WGA fluorescence signal was averaged across the cell width to obtain a line profile of intensity along the cell length. The peaks, corresponding to the septa, were identified using a custom peak-finding algorithm in MATLAB, and the changes in wall lengths were calculated from the peak-to-peak separations. All data were manually curated to ensure accuracy.

Transmission EM preparation

For transmission EM (TEM), liquid cultures of *B. subtilis* 168 were grown in LB or MM and then harvested during exponential growth (OD_{600} = 0.3–0.5 in LB; OD_{600} = 0.05–0.08 in MM) by centrifugation at 3500 × *g*. The sample preparation protocols for cells grown in LB and MM were identical. All reagents were obtained from Electron Microscopy Sciences (Hatfield, PA) and all treatments were performed at room temperature unless otherwise specified. Cells were fixed by suspending the pellet in 6 mL of 0.1 M sodium cacodylate buffer with 2% formaldehyde and 4% glutaraldehyde (pH 7.3) for 1 hr. Cells were centrifuged at 3500 × *g* for 10 min and washed by resuspending the pellet in 6 mL of 0.1 M sodium cacodylate buffer for 5 min. The washing step was repeated three times with fresh buffer and the resulting pellet was suspended in 100 μL 10% gelatin in PBS that was preheated to 37°C. Cells were centrifuged at 3500 × *g* before the gelatin solidified. Immediately after centrifugation, the pellet was put on ice for 10 min, overlaid with 100 μL of the fixative, and stored overnight at 4°C.

The pellet was then extracted and cut into four pieces to increase the surface area. Each piece was separately stained with 500 μL 1% osmium tetroxide in Milli-Q water for 1 hr at 4°C with shaking. Samples were then washed three times with fresh Milli-Q water at 4°C for 15 min and stained with 500 μL 1% uranyl acetate for 8 hr at 4°C with shaking. The samples were then dehydrated by shaking successively in 1 mL of 50% and 70% (w/v) ethanol at 4°C for 15 min each. Further dehydration was

achieved by shaking successively in 1 mL of 95% and 100% (w/v) ethanol for 15 min each. The samples were then shaken in 1 mL 100% propylene oxide for 30 min to substitute ethanol with propylene oxide. Infiltration of the samples by epon was achieved by first shaking in a 50% solution (w/v) of epon in propylene oxide for 1 hr, followed by overnight shaking in a 67% solution (w/v) of epon in propylene oxide. The samples were then embedded into molds filled with 100% epon and allowed to settle for 4 hr to let the remaining propylene oxide escape. The molds were baked overnight at 65°C to harden the epon.

Serial, ultrathin sections (80 nm) of the embedded samples were cut with a glass knife made with a Leica EM KMR2 glass-knife maker using a Leica EM FCS ultramicrotome (Leica Microsystems, Wetzlar, Germany) and collected on 100 mesh-size formvar carbon grids. While on the grids, the sections were stained with a 1:1 mixture of 100% uranyl acetate and 100% ethanol for 20 min, followed by rinsing with Milli-Q water. The sections were further stained with 0.2% lead citrate for 5 min in the presence of sodium hydroxide pellets to absorb CO_2. Finally, the sections were rinsed with water and dried before they were imaged on a JEM-1400 transmission electron microscope (JEOL, Tokyo, Japan).

Computational analysis of TEM cell-wall cross-sections

Cell walls from TEM images were traced using a custom algorithm in MATLAB similar to bacterial cell midline-detection algorithms (9). The negative of the image was contrast adjusted and median filtered to avoid sharp local gradients. Tracing of the cell-wall centerline was initiated at two user-determined initial locations within the cell wall ($\mathbf{r}_0$ and $\mathbf{r}_1$) ~10 nm apart that provided the trial starting point ($\mathbf{r}_0$) and the trial tangent direction ($\mathbf{r}_1 - \mathbf{r}_0$). A linear segment $L \sim 50$ nm in length and perpendicular to the trial direction was drawn through $\mathbf{r}_1$. The intensity-weighted center point ($\mathbf{r}_c$) was computed along this segment using

$$\mathbf{r}_c - \mathbf{r}_0 = \frac{1}{N}\sum_{s=1}^{N}(\mathbf{r}(s) - \mathbf{r}_0)\frac{Z(s)}{\max(Z)}, \quad (2)$$

where s is the index of points from one end of the line segment, N is the total number of points between the two ends of the segment, and $Z(s)$ is the local image intensity along s. A new trial tangent direction was defined by $\mathbf{r}_c - \mathbf{r}_0$ and a new center point was iteratively determined until its position converged. The next trial point was determined by moving 10 nm along the trial tangent. This process was repeated until a user-defined end-point along the cell wall was reached. Linear sections perpendicular to the centerline running through points along the centerline spanning ~50 nm in length were used to define smooth intensity profiles. The points of maximum derivative of the resulting profile were used to define the inner and outer edges of the wall, and the distance between these points defined the wall thickness. The thickness of each cell wall was measured at 150–350 separate positions, depending on the quality of the micrograph, to estimate the mean thickness and the SD.

Computational model of elongation

Simulations were initiated by relaxing two layers of effective springs, connected only at the ends, under a constant extensional force F acting on the cell endcaps representing turgor pressure. Each effective spring represents the combination of all peptides around the circumference at a given position along the longitudinal axis of the cell. The effective spring constant of the i^{th} layer is given by

$$K_i = \left(\sum_j \kappa_{ij}^{-1}\right)^{-1}, \quad (3)$$

where κ_{ij} is the spring constant of the j^{th} spring in the i^{th} layer. The energy of the spring network is thus given by

$$E = \frac{1}{2}\sum_i K_i(l - \eta_i d)^2 - Fl, \quad (4)$$

where η_i is the number of springs in the i^{th} layer, $d = 1$ nm is the rest length of each spring, and l is the length of the cell excluding the end caps. For a given network, the energy was minimized to obtain the cell length at mechanical equilibrium.

Under the approximation of uniform strain across the cell wall, the longitudinal stress is given by $\sigma = \Pi A_c/A_w$, where Π is the turgor pressure, $A_c = \pi r^2$ is the cross-sectional area of a cell of radius r, and $A_w = 2\pi r d$ is the cross-sectional area of a cell wall of thickness d. For $\Pi = 15$ atm, $r = 0.5$ μm, and $d = 30$ nm, $\sigma = 125$ atm. To parameterize the spring constant of an individual effective spring, we estimate the spring constant of the entire wall as $\kappa_w = YA_w/l$, where $Y \approx 50$ MPa is the Young's modulus (18,31) and l is the cell length. The relaxed length of a peptide cross-link is ≈ 1 nm, and thus the number of cross-links per μm is $n_p \approx 1000$. Because different layers act together to resist turgor forces, the average stiffness of each peptide is $\bar{\kappa} = n_p l\kappa_w/N = n_p YA_w/N \approx 225$ N/m, where N is the total number of layers. However, this relation must be modified to account for variability in the number of springs and spring constants in each layer; the initial spring constant κ_0 must be larger than the average $\bar{\kappa}$ to account for hydrolysis. Therefore, we set $\kappa_0 = 400$ N/m, which yields a Young's modulus of 50 MPa in our simulations.

New layers were synthesized at a rate k_s. To mimic the removal of individual cross-links due to hydrolysis and/or bond rupture, all effective springs were progressively dissolved by reducing their spring constant at a rate k_h. An effective spring was considered completely dissolved when its spring constant reached zero. In cases in which we included insertion within the innermost layer, the rate of insertion of new springs was $k_i\eta_1$, where η_1 is the number of springs in the innermost layer. The spring constant of newly inserted springs was initialized at κ_0. During each time step ($dt = 20$ s), we adjusted the network architecture and spring constants according to the rules described above and then relaxed the network according to Eq. 4. After the network reached a steady-state wall thickness, we set the turgor force $F = 0$. As a result of the removal of turgor pressure, the network shrank from its extended length, l, to a new equilibrium length, l_{gl}, at which the inner layers were compressed while the outer layers were under tension. We then calculated the global strain as $\gamma_{gl} = (l - l_{gl})/l_{gl}$.

RESULTS

Single-cell quantification of the elongation rate, cell-wall thickness, and global strain of *B. subtilis* cells

Using phase-contrast microscopy, we measured the width of *B. subtilis* cells at subpixel resolution during exponential growth in both LB and MM (see Materials and Methods). In both media, we found that the width variability was small (Fig. S1 in the Supporting Material), illustrating that elongation is the primary result of growth. To constrain models of Gram-positive bacterial elongation, we sought to experimentally measure three key quantities: the relative elongation rate, cell-wall thickness, and global strain. We measured these quantities for *B. subtilis* 168 cells in LB and MM. We chose media with substantially different compositions to uncover general growth behaviors. Using time-lapse imaging in a microfluidic flow chamber (see Materials

and Methods), we measured the rate of elongation $v = dl/dt$, where $l(t)$ is the length of the cell as a function of time. The cells elongated exponentially, and hence the relative growth rate v/l was constant in time (independent of length for an individual cell); a doubling time of 20 min is equivalent to $v/l = 3.5 \times 10^{-2}$ min^{-1}. In LB, we observed $v/l = 3.6 \pm 0.8 \times 10^{-2}$ min^{-1} (Fig. 1 *A*). As expected, the relative elongation rate was substantially reduced in MM ($1.2 \pm 0.2 \times 10^{-2}$ min^{-1}, corresponding to a doubling time of ~60 min; Fig. 1 *A*).

To investigate whether changes in growth rate were reflected in changes to the mechanical state of the cell wall, we measured the global strain by releasing the turgor on the cell wall through osmotic up-shock (see Materials and Methods, Fig. 1 *B*, and Fig. S2 *A*). The global strain for exponentially growing cells was 0.26 ± 0.04 in LB and 0.22 ± 0.03 in MM (Fig. 1 *C* and Fig. S2 *B*), indicating that the wall is stretched by similar amounts in the two media. Phase and fluorescence images yielded strain values in agreement to within 3% (Fig. S2 *C*), indicating that the cytoplasm and cell wall experienced the same reduction in strain. This strategy was previously applied to study the response of Gram-negative *E. coli* cells to hyperosmotic shock (32,33) and produced global strain estimates of the same magnitude (~10–20%) as our data for *B. subtilis*.

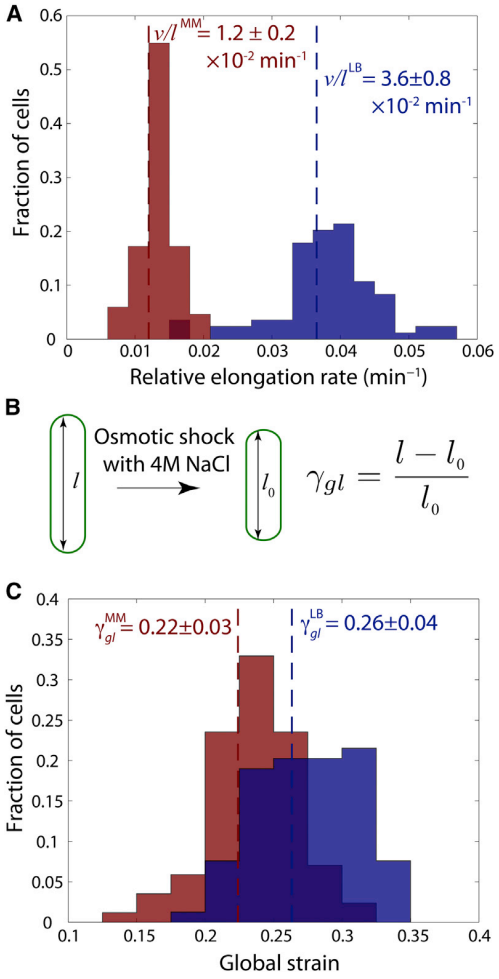

FIGURE 1 The relative elongation rate decreases threefold in MM relative to LB, whereas global strain is maintained. (*A*) Histograms of relative elongation rate (v/l) of *B. subtilis* 168 cells in LB (*blue*, $n = 84$ cells) and MM (*red*, $n = 153$ cells). (*B*) Schematic of the osmotic shock process used to measure global strain. (*C*) Histograms of global strain (γ_{gl}) of *B. subtilis* 168 in LB (*blue*, $n = 79$ cells) and MM (*red*, $n = 85$ cells).

In a previous study, Matias and Beveridge (21) estimated the thickness of the *B. subtilis* cell wall at ~30–40 nm using cryo-EM. Intriguingly, they also reported that the variability of the thickness across cells was small (~10–20%). To determine whether the steady-state wall thickness is uniform within individual cells, we performed TEM on exponentially growing cells in LB and MM, and developed computational methods to measure the thickness profiles of individual cell walls (see Materials and Methods) (9). The thickness profiles of cells grown in LB were reasonably uniform within single cells (<8% variation; Fig. 2, *A* and *B*), and the variability of the average thickness across cells was also low (31 ± 2.5 nm or ~20 layers, $n = 55$ cells). For cells grown in MM, thickness was similarly uniform both within cells (<11%) and across cells (28.5 ± 3 nm, $n = 37$ cells). The agreement between the two media conditions in terms of wall thickness and global strain suggests that the mechanism of *B. subtilis* elongation produces a cell wall whose thickness and strain are insensitive to the rate of elongation. The contrast between the wall and surrounding material was lower in images of cells grown in MM compared with LB. This difference could be due to factors such as the density of teichoic acids or other proteins intercalated within the wall, the density of the wall itself, or the staining efficiency. Nonetheless, we could easily detect a sharp change in density that we interpreted as corresponding to the edges of the wall, and therefore computationally measured wall thickness using the same algorithm in both media (see Materials and Methods). Thus, we sought to identify biophysical growth models that yield relatively constant wall thickness and strain across a wide range of growth rates to simulate growth in LB and MM.

Biophysical model of rod-shaped Gram-positive cell-wall elongation

In the rod-shaped Gram-negative bacteria *E. coli* and *Caulobacter crescentus*, cryo-electron tomograms of isolated cell walls have indicated that the glycan strands are oriented approximately circumferentially and are connected by longitudinally oriented peptide cross-links (34). Although the details of the architecture of Gram-positive cell walls are not known, atomic force microscopy has suggested that glycans also have a circumferential organization in *B. subtilis* (35) and *Lactobacillus helveticus* (16). Thus, we constructed a minimal model of a Gram-positive cell

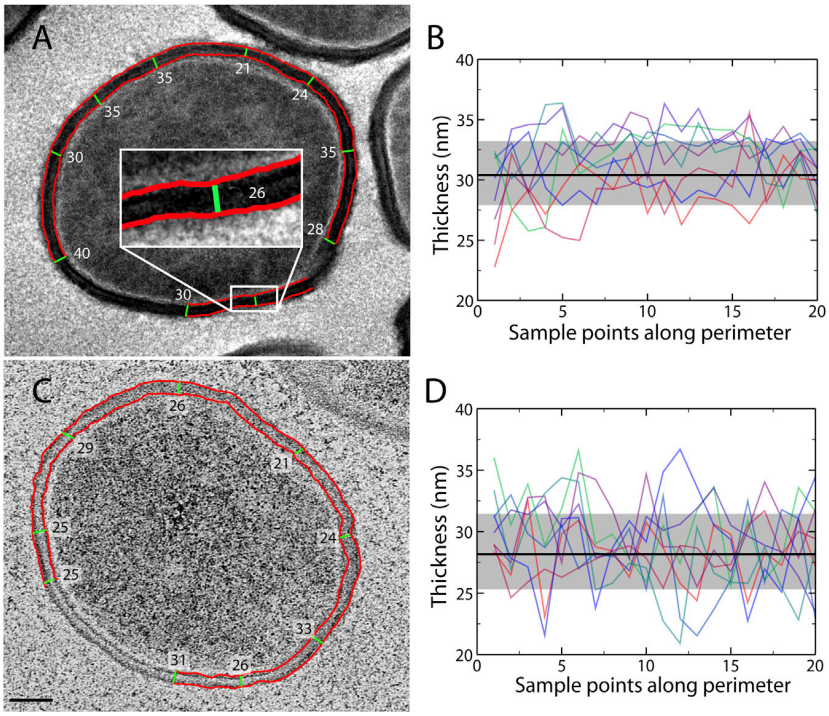

FIGURE 2 Cell-wall thickness is maintained within cells and across growth conditions. (*A* and *C*) Representative TEM cross-sections of cells grown in LB (*A*) and MM (*C*), with computationally detected boundaries (*red*) and thickness measurements (*green*) separated by at least 100 nm. Although the walls did not stain with as much contrast in MM as in LB, the borders were easily detected. Numbers label the thickness of the wall at the adjacent green lines. Scale bar: 100 nm. (*B* and *D*) Average cell-wall thickness (*solid black*) and mean ± 1 SD (*gray rectangle*) for cells grown in LB ($n = 55$) and MM ($n = 37$). A random subset of thickness profiles from eight cells is shown in each panel, demonstrating the low variability within individual walls.

wall as a multilayered network of springs (Fig. 3 *A*). We assume that the stiff glycans are oriented circumferentially and thus act mainly to determine the cell width. We then model peptide cross-links as Hookean springs oriented along the longitudinal axis that act as the primary stress-bearing components resisting turgor-driven elongation (Fig. 3 *A*).

Although growth likely introduces heterogeneity into the wall architecture, we found using phase-contrast microscopy that *B. subtilis* cells can nevertheless maintain their shape and width in a variety of growth conditions (Fig. S1). Therefore, to focus on elongation dynamics, we assume that each layer within the peptidoglycan architecture can be treated as homogeneous in the circumferential direction and along the cell length, thereby decoupling longitudinal and radial expansion. Thus, we replace the two-dimensional cylinder of springs comprising each layer with a line of identical, effective springs, each of which represents the summed contributions of all springs around the circumferential direction at a particular position along the cell length, with a spring constant κ that can be different for each layer (Fig. 3 *A*). We initially assume that the wall is comprised of layers of peptidoglycan that are laid down sequentially during growth, and later introduce progressive insertion within an existing layer. The layers are connected by the polar endcaps that transmit the turgor pressure to the wall in the longitudinal direction and constrain all layers to have the same length. We assume that the endcaps play no active role in elongation mechanics, since experimental observations indicate that the poles have much slower turnover of wall material than the cylindrical region (20,36). Therefore, at any particular time in our simulations, the cell wall is characterized simply by the number of springs in each layer and their spring constant, and the overall cell length.

We assume that new layers are synthesized at a rate k_s in an unstressed state with enough springs to precisely span the length of the cell at the time of synthesis. Importantly, the addition of a new, unstressed layer alone does not perturb the mechanical equilibrium of the existing layers and therefore does not affect the cell length, indicating that a second biochemical process is required to perturb the distribution of stresses within the cell wall network. One possibility is the removal of cross-links, which can occur either through enzymatic action by hydrolases or through bond rupture at high strain. For simplicity, we focus on a model in which peptides are removed at a constant rate k_h throughout the wall; we will refer to this process as hydrolysis for the remainder of the text. As the layers undergo hydrolysis, the effective spring constants decrease linearly with a rate $d\kappa/dt = -k_h$ until they reach zero, signifying that the layer is lost because it can no longer bear any stress. The decreasing spring constants lead to the further extension of all layers. The thickness of the wall is defined as the number of layers with nonzero spring constant. In the limit of extremely fast hydrolysis, the cell wall will disintegrate because a new layer will be completely hydrolyzed before the next layer is synthesized. However, for moderate values

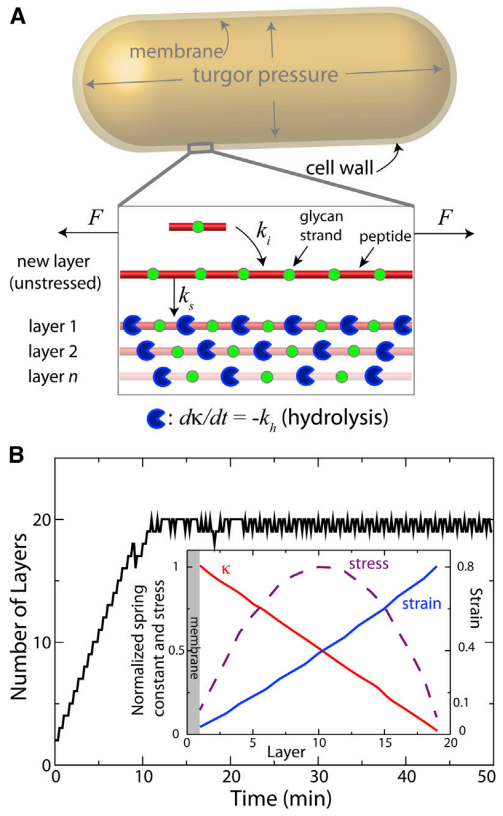

FIGURE 3 Model for Gram-positive cell-wall elongation through balance between synthesis and turnover. (*A*) The membrane transfers force due to turgor pressure onto the cell wall, which is assumed to have a multilayered structure (zoomed-in cross-section shown in *rectangle*). The stiff glycan strands (*green circles*) are oriented along the circumference perpendicular to the long axis of the cell, and the peptide bonds connecting the strands are oriented parallel to the long axis (*red cylinders*). In our model, each peptide is an effective spring representing the summation of restoring forces from all cross-links around the circumference. New, unstressed layers are added at a rate k_s. Material can also be inserted within the existing innermost layer at a rate k_i, thereby compressing the layer. All layers are subject to hydrolysis that reduces the peptide spring constant κ with a rate $-k_h$, and to a longitudinal extensional force F borne primarily by the peptides. The layers are connected at the poles by the end caps. (*B*) Results from simulation of growth with $k_s = 1.2\ \text{min}^{-1}$, $k_h = 0.06\ \text{min}^{-1}$, $k_i = 0$, and turgor pressure $\Pi = 15$ atm. Inset: Normalized values of the steady-state spring constant and stress, and absolute values of the strain across the layers. The middle layers bear most of the extensional stress.

of k_h, this framework qualitatively matches the inside-to-outside growth mechanism proposed by Koch (19) and Koch and Doyle (20): it results in a progressive movement of layers away from the membrane and eventually complete loss of material composing a layer (Fig. 3 *B*), which is balanced by the synthesis of new layers.

The biophysical parameter in our model characterizing wall stiffness is the effective spring constant of a newly synthesized layer κ_0, whose value we chose to yield the measured *B. subtilis* cell wall Young's modulus of 50 MPa (14,15,37) (see Materials and Methods for more details). Previous experiments indicated that the time interval from incorporation of radiolabeled peptidoglycan precursors into the wall until the first release of the isotope is approximately one doubling time (20 min for growth at 37°C in LB) (20). Therefore, for a cell wall with ~20–30 layers of thickness ~1 nm, the cells must be laying down layers at a rate $k_s \sim$ 1–1.5 layers per minute.

To determine whether our model permits a steady-state wall thickness, we performed simulations of the elongation dynamics of a multilayered cell wall for the experimentally motivated synthesis rate $k_s = 1.2\ \text{min}^{-1}$, and a hydrolysis rate $k_h = 0.06\ \text{min}^{-1}$ selected to produce a doubling time of ~20 min. To challenge the system to achieve a steady state, we initialized the network with two layers and allowed the network to relax under the applied extensional load of a turgor pressure $\Pi = 15$ atm (7). The thickness stabilized at a steady-state value of 20 layers on the timescale of doubling, as expected since the spring constant of each layer decreases to zero with a regular time constant proportional to $1/k_h$. At steady state, we found that the strain of a given layer increased linearly with its distance from the membrane (reflecting its age), with a corresponding linear decrease in the spring constant (stiffness; Fig. 3 *B*, *inset*). The outermost layers were too soft to contribute significantly to stress bearing, and the newest layers were not yet extended enough to absorb significant amounts of the stress. The competition between these two trends led to the middle layers bearing most of the stress (Fig. 3 *B*, *inset*). The model also predicted an exponential elongation of the cell length at steady state, since new layers are being synthesized with a surface area proportional to the length of the cell and hydrolysis occurs at a constant rate for all wall material.

Even though different layers experienced different strains at steady state, the fact that they were constrained to have the same length by virtue of being connected by common endcaps dictated an overall extensional strain in the wall due to turgor pressure. We define this wall property as the global strain $\gamma_{gl} = l/l_{gl} - 1$, where l is the extended length under turgor pressure and l_{gl} is the equilibrium length for zero turgor pressure at which the inner layers are compressed and the outer layers are under tension (Fig. S3). The global strain is proportional to the turgor pressure and inversely correlated with the wall spring constant κ_0.

Proportional synthesis and turnover decouples wall thickness and growth rate

We comprehensively explored the minimal model described in Fig. 3 across all values of the parameters k_s and k_h (Fig. 4), and found that there is a region of parameter space that simultaneously fits our experimental data in LB for wall thickness (Fig. 4 *A*), growth rate (Fig. 4 *B*), and global strain (Fig. 4 *C*). Because k_s sets the timescale for the appearance of new layers and k_h sets the timescale for a newly inserted effective spring to dissolve completely, the steady-state

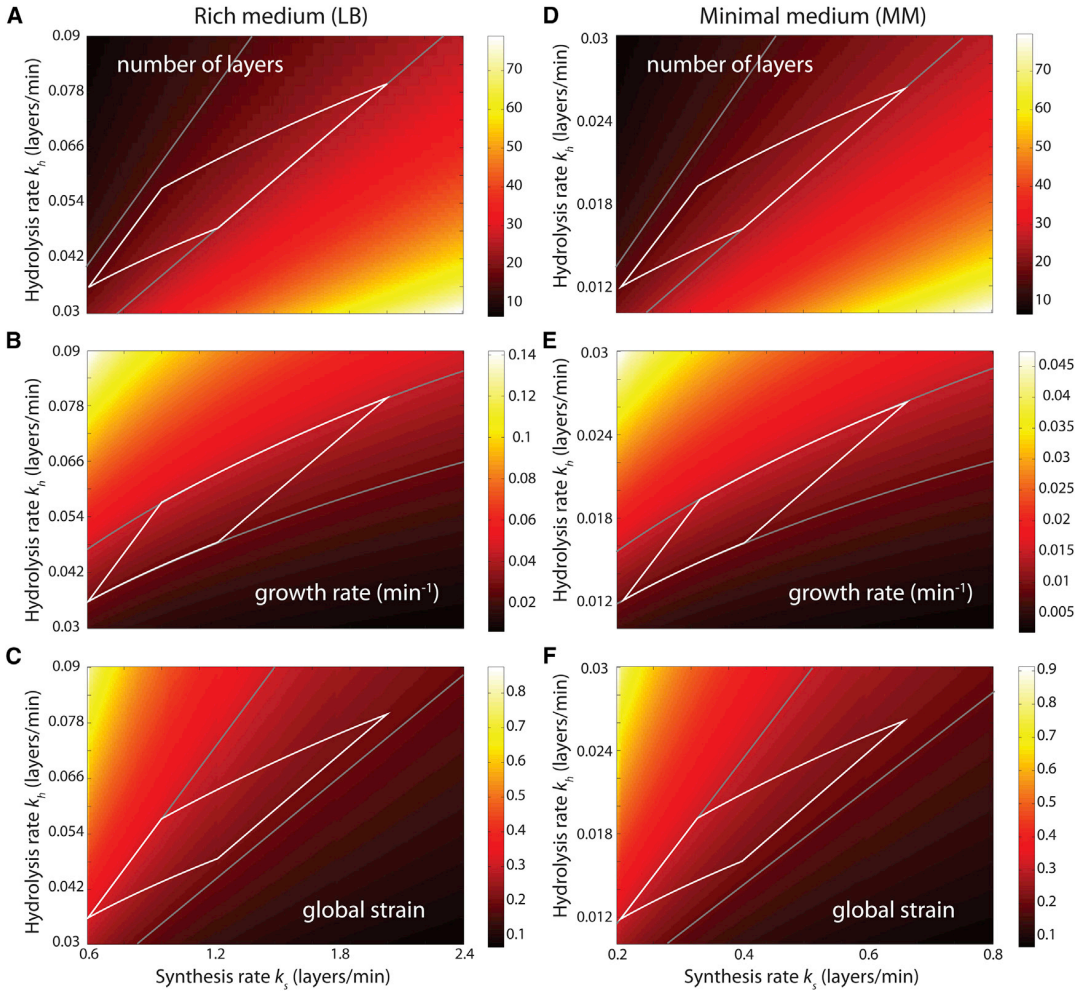

FIGURE 4 Model predictions for cell-wall properties are consistent with experimental data in both LB and MM. (*A–C*) We used simulations to predict the steady-state number of layers comprising the cell wall N (*A*), the relative elongation rate v/l (*B*), and the global strain γ_{gl} (*C*). The gray lines outline a region of parameters consistent with each of our experimental measurements individually: (*A*) $N = 20 \pm 5$, (*B*) $v/l = 3.6 \pm 0.8 \times 10^{-2}$ min^{-1}, and (*C*) $\gamma_{gl} = 0.25 \pm 0.05$. The white quadrilateral represents the overlap of consistency regions in *A–C* in which the values of k_s and k_h simultaneously reproduce all three experimental measurements. (*D–F*) Based on our observation that growth rate decreased threefold in MM, we scaled the range of values of k_s and k_h by threefold. Gray lines and white regions represent consistency with experimental measurements in MM: (*D*) $N = 20 \pm 5$, (*E*) $v/l = 1.2 \pm 0.3 \times 10^{-2}$ min^{-1}, and (*F*) $\gamma_{gl} = 0.25 \pm 0.05$. The turgor pressure and Young's modulus are held constant in all simulations at $\Pi = 15$ atm and $Y = 50$ MPa, respectively.

number of layers N scales linearly with the ratio k_s/k_h (Fig. 4 *A*). In contrast, the growth rate v/l scales with $1/k_s$ because every new layer strengthens the cell wall and allows the cell to resist expansion due to turgor pressure. The growth rate scales quadratically with k_h^2 because an increase in hydrolysis weakens the wall not only by weakening the springs within each layer but also by reducing the steady-state thickness of the wall (Fig. 4 *B*). This provides a qualitative description of why growth rate can increase if both wall synthesis and turnover rates increase.

We can make these heuristic scalings concrete by using a continuum model of cell-wall density in which we assume that new layers are synthesized at a rate k_s in an unstressed state spanning the length of the cell at the time of synthesis. Each layer can be characterized by its length l, relaxed length l_0, and an extensional strain $\gamma = l/l_0 - 1$ that we now assume is smoothly varying across layers. Therefore, the wall can be characterized by the time-dependent density of layers $n(\gamma, t)$ with strain between $[\gamma, \gamma + d\gamma]$, with k_h as the rate of cell-wall material removal (e.g., due to hydrolysis). The function n does not represent the density of material within individual layers, but rather is a convenient representation of the state of the cell wall across its thickness that can be used to calculate the total number of layers, as we demonstrate below. Here, we assume that k_h is constant across all layers and in time. All layers with strain $\gamma - d\gamma$ at time $t - dt$ will extend to have strain γ in a time interval dt; thus, the evolution of $n(\gamma)$ is given by

$$n(\gamma, t) = n(\gamma - d\gamma, t - dt) - k_h n(\gamma, t) dt. \quad (5)$$

The steady-state density $n(\gamma)$ at which $\partial n(\gamma,t)/\partial t = 0$ determines the steady-state wall thickness. To solve for $n(\gamma)$, we expand Eq. 5 to first order in γ and t, giving

$$\frac{\partial n(\gamma)}{\partial \gamma} = -\frac{k_h n(\gamma)}{d\gamma/dt}. \quad (6)$$

The strain rate is related to the velocity of the cell ends v by the relation $d\gamma/dt = 1/l_0(dl/dt) = v(\gamma+1)/l$; inserting into Eq. 6 gives

$$\frac{dn(\gamma)}{n} = -\frac{lk_h}{v}\frac{d\gamma}{1+\gamma}. \quad (7)$$

Note that Eq. 7 holds generally for k_h replaced by any choice of peptide-removal function $k_h(\gamma)$ that is dependent only on strain.

The steady-state density can be determined by integrating Eq. 7 from 0 to γ, giving

$$n(\gamma) = n_0\left(\frac{1}{1+\gamma}\right)^{\alpha}, \quad (8)$$

where n_0 is the layer density at $\gamma = 0$, and $\alpha = k_h l/v$. Note that for $n(\gamma)$ to be time independent, α and hence l/v must also be time independent. Therefore, the exponential growth law $v = dl/dt \propto l$ follows naturally from our analysis. To solve for α and n_0, we apply the mass and force balance constraints

$$k_s = \int_0^{\infty} k_h n(\gamma) d\gamma, \quad (9)$$

$$\frac{\sigma}{Y} = \int_0^{\infty} \gamma n(\gamma) d\gamma, \quad (10)$$

where $\sigma = \Pi A_c/A_l$ for turgor pressure Π, cellular cross-sectional area A_c, and unit layer cross-sectional area A_l, and Y is the Young's modulus of the wall material. In Eq. 9, synthesis of new layers is balanced by the combined removal of layers, giving

$$\frac{k_s}{k_h} = n_0\frac{1}{\alpha-1} \Rightarrow \alpha = 1 + n_0\frac{k_h}{k_s}. \quad (11)$$

For Eq. 10 to be integrable, $\alpha > 2$ is required, thereby setting a lower bound $k_h > 2v/l$. We can solve for n_0 from Eq. 10, giving

$$\frac{k_h^2}{k_s^2}\frac{\sigma}{Y}n_0 = 1 + \frac{k_h}{k_s}\frac{\sigma}{Y} \Rightarrow n_0 = \frac{Y}{\sigma}\frac{k_s^2}{k_h^2} + \frac{k_s}{k_h}. \quad (12)$$

The steady-state cell-wall thickness is

$$N = \int_0^{\infty} n(\gamma) d\gamma = \frac{k_s}{k_h}, \quad (13)$$

and the doubling time is

$$\frac{l}{v}\ln 2 = \left(\frac{2}{k_h} + \frac{Yk_s}{\sigma k_h^2}\right)\ln 2. \quad (14)$$

We can also solve for the global strain within a wall of length l by using $1+\gamma = l/l_0$ to rewrite $n(\gamma)$ as

$$n(l_0) = n_0\left(\frac{l_0}{l}\right)^{\alpha} \quad (15)$$

for $l_0 < l$. When the turgor stress σ is set to zero, all layers adopt a length l_{gl} that satisfies Eq. 10, which yields the global strain

$$\gamma_{gl} = \frac{l}{l_{gl}} - 1 = \frac{1}{\alpha-2} = \frac{\sigma}{Y}\frac{k_h}{k_s}. \quad (16)$$

Thus, N and γ_{gl} have the same k_h/k_s scaling.

For a cell wall mimicking *B. subtilis* with $N \approx 20$, $l/v\ln 2 \approx 20$ min, and $Y/\sigma \approx 0.35$, we can then estimate $k_s \approx 6/\text{min}$ and $k_h = 0.3/\text{min}$ from Eqs. 13 and 14. Using these values, we obtain an estimate of $\gamma_{gl} \approx 0.15$ that matches reasonably well with our experimental measurements (Fig. S4). This agreement indicates that our quantitative measurements of global strain are consistent with our predictions based on measured values of the Young's modulus of the *B. subtilis* cell wall (18,31), providing further evidence of the mechanics of growing *B. subtilis* cells. Thus, our continuum model is a powerful tool that can also be applied to more complex biochemical models of cell-wall synthesis and turnover.

The scaling of N with k_s/k_h indicates that thickness is preserved if k_s varies proportionally with k_h. Given that the cell-wall thickness in LB is maintained in MM, the scaling of v/l with k_h^2/k_s indicates that a threefold change in growth rate can be achieved without affecting thickness by reducing both k_s and k_h by a factor of 3. Indeed, simulations based on our discrete model predict that the thickness will be unchanged upon a threefold reduction of k_s and k_h (Fig. 4 *D*), whereas the growth rate will experience a threefold reduction (Fig. 4 *E*). Our model then predicts that the global strain in MM will be very similar to that in LB (Fig. 4 *F*), consistent with our experimental observations. An alternative explanation for the reduction in growth rate in MM would be an ~3-fold reduction in the turgor pressure. However, in that scenario, the global strain would decrease by a similar factor, contrary to our experimental measurements (Fig. S5). Although we cannot exclude the possibility that in MM there is a lower turgor pressure that nevertheless produces similar global strain due to certain details of wall

mechanics, such as nonlinear responses not included in our model, our data nevertheless suggest that *B. subtilis* cells maintain the same turgor pressure in LB and MM, based on our experimental determination that wall thickness and strain are maintained. Taken together, our findings suggest that elongation results from the competing effects of cell-wall synthesis and hydrolysis, with the reduction in growth rate in MM potentially resulting from a similar scaled decrease in both synthesis and hydrolysis rates.

DISCUSSION

We have presented a minimal, mechanochemical model of Gram-positive cell-wall elongation that accurately predicts the relationships among growth rate, cell-wall thickness, and strain. In our model, turgor pressure plays a major role in determining the growth rate and the global strain, whereas the wall thickness is roughly independent of turgor pressure. In particular, the model explains how *B. subtilis* cells can maintain their wall thickness and global strain while growth rate is reduced threefold. To achieve this, cells can downregulate wall synthesis and hydrolysis proportionally while maintaining a constant turgor pressure. This also indicates a means by which *B. subtilis* cells can leverage control over wall synthesis and hydrolysis rates by regulating the expression of precursors and hydrolases to shift wall thickness and growth rate independently of each other. These conclusions provide motivation for future explicit quantitative measurements and perturbations of the rates of synthesis and hydrolysis, and for direct measurements of turgor pressure. In comparing growth in MM and LB, our intention was to determine whether cell-wall properties could be maintained despite the large metabolic and growth differences between the two media. The development of a high-throughput method for measuring cell-wall thickness would allow for a more comprehensive exploration of growth in other media, temperatures, and Gram-positive species.

Our results make several explicit predictions that warrant further experiments: 1), the strain is greatest in the outermost intact layer; 2), the stress is greatest in the middle layers (Fig. 3 *B*) (20); and 3), as a result, a small patch of material excised from the wall of an elongating cell would have an asymmetric stress distribution across the wall thickness upon removal of turgor pressure (Fig. S3), and hence could adopt a nonplanar geometry that could be observed by EM. Moreover, any hydrolases that are not covalently anchored to the membrane and/or wall could be lost to the extracellular environment after unbinding from a site of activity. In this case, nearby cells in a densely packed community could also capture these lost hydrolase molecules and use them to speed up growth, at the cost of weakening their walls. Similar sharing of metabolic enzymes within a community of tens of cells has been shown to accelerate growth in budding yeast (38).

In addition to our own data, our model captures several phenomena previously reported in the literature. Our model supports the hypothesis that controlled degradation of the cell wall is necessary for normal elongation of *B. subtilis* cells, and that growth can be accelerated by increasing the rate of hydrolysis (22). Consistent with the inverse relationship between growth rate and wall thickness predicted by our model, a temperature-sensitive mutant with impaired autolysin activity was previously shown to have a slower growth rate and thicker wall than wild-type cells (22). Moreover, the addition of lysozyme or purified *B. subtilis* autolysin increased growth rate (22) and reduced the wall thickness (39), as would be predicted by our model with an increase in k_h. This intriguing behavior has nontrivial implications for the effects of treating Gram-positive bacteria with sublethal concentrations of molecules that degrade the existing cell-wall material and hence could increase the rate of elongation and even proliferation. However, cells that have increased growth rate at the cost of having a thinner, softer cell wall may be more susceptible to lysis due to osmotic shock or other mechanical perturbations.

In a recent study, Dyson et al. (40) developed a mathematical model of plant cell-wall elongation that has many characteristics in common with our model. In brief, it formulates the osmotic-pressure-driven deformation of the plant cell wall in response to enzymatic cleavage of flexible, longitudinally oriented hemicellulose polymers. Like our model, their model predicts that stress is maximal in the middle layers of the cell wall, suggesting that this may be a general property of inside-out growth mechanisms in which wall material is deposited on the inside of the wall at zero stress, and is then continually stretched as it is advected toward the outer surface of the wall as it is hydrolyzed. On the other hand, their model imposes a constant wall thickness, whereas we allow synthesis and consequently wall thickness to be a free parameter, which allows us to validate our model by fitting the experimentally observed wall thickness. Finally, their model includes a term that describes nonlinear, stretch-induced breakage of the load-bearing elements, which may be necessary to attain a theoretical yield stress (a stress below which the wall does not expand). This has long been known to be a mechanical property of the plant cell wall, although it has not yet been observed in prokaryotes.

The coupling between peptidoglycan hydrolysis and synthesis is not well elucidated in the literature due to the large number of enzymes that participate in each process and the presumed regulatory complexity. However, our model provides a simple mechanical picture of elongation, without requiring elaboration of the specifics of the molecular machinery, that suggests how synthesis and hydrolysis of the cell wall may be linearly coupled to maintain wall thickness and global strain. Recent experiments showed that the dynamics of the cytoskeletal protein MreB can be rapidly arrested in *B. subtilis* with the use of antibiotics such as

vancomycin (41,42). In those experiments, the cell wall continued to expand around the MreB fluorescence density for ~30 s to 1 min after MreB motion arrest (41). A simple interpretation of this transient behavior is that hydrolysis continued, softening the cell wall and permitting continued elongation due to turgor pressure. However, the fact that cells can avoid lysis even when wall synthesis has been stopped indicates that the cell must employ a currently unknown mechanism to shut off hydrolysis.

Although our minimal model successfully predicted our experimental measurements of growth rate, wall thickness, and global strain, it can also easily be modified to capture other processes, such as bond rupture at high strain, or localized or strain-dependent hydrolase activity. Lower hydrolysis rates in layers that are relatively unstrained (e.g., due to reduced hydrolase binding) could provide a buffer against lysis for fast-growing cells. In this scenario, we speculate that mechanics could also provide feedback for biochemical regulation. For example, a growing cell subject to compression from the surrounding microenvironment could experience a reduction in growth rate due to less turnover as the effective hydrolase concentration in the cell increases, and this increase could be used as a chemical signal. Moreover, we have considered the effects of inserting peptidoglycan in localized bursts in addition to layers. Our simulations indicate that including insertion of peptidoglycan patches into the newest, mostly unstressed layer of the wall does not significantly affect the predicted dimensions or growth rate of the cell (Supporting Material; Fig. S6). Currently, our model assumes a circumferential organization of the glycan strands and a layered structure. Recent results from atomic force microscopy suggested that Gram-positive cell walls may have a more complex three-dimensional architecture (16,35), although it is not clear how the stress-bearing elements of such a network would be oriented. Future studies examining the architecture of Gram-positive cell walls will provide the opportunity to refine our model by highlighting other experimental measurements that can act as constraints.

Based on our findings of low variability in cell width within and across single cells (Fig. S1), we assumed that each layer is homogeneous, and hence focused only on the mean thickness of the wall. However, our discrete model can easily be modified to account for heterogeneity within each layer, and future implementations will focus on variability in wall thickness, such as the nutrient-dependent changes in septal wall thickness observed in the round Gram-positive bacterium *Staphylococcus aureus* (43). Here, we assumed a constant rate of hydrolysis for all cross-links; we note that the decreasing number of bonds in each layer moving outward from the membrane indicates that the total amount of hydrolysis per unit time is lower in layers farther from the membrane, consistent with a morphogen-like gradient of hydrolase molecules produced at the membrane that then diffuse throughout the wall and are captured. A full exploration of the extent to which spatial- and strain-dependent hydrolysis affects the state of the wall will be the subject of future investigation.

In summary, we have developed a model for the mechanics of elongation in *B. subtilis* that successfully predicts a conserved wall thickness and global strain in LB and MM, and suggests that a coincident threefold reduction in both synthesis and hydrolysis can yield our observed threefold reduction in growth rate in MM relative to LB. The maintenance of wall thickness and global strain between these conditions indicates that the cell wall has similar local architectures and distributions of stress in the two growth conditions. If this similarity exists across other growth media, it may allow cells to transition more easily between different environments, because the cells would not be any more susceptible to mechanical perturbations in one medium than in another. Maintenance of thickness even under nutrient-poor conditions suggests that wall integrity is a high priority, supporting the notion that cell-wall pathways are critical for both shape maintenance and survival. Finally, the recurrent theme of coupled synthesis and hydrolysis in both elongation and sporulation suggests that these processes generate mechanical forces that can be transduced by the cell for a variety of morphogenetic programs that should serve as the basis of future modeling research, with the cell-wall growth machinery acting as a type of motor that can drive not only proteins but also cellular-scale structures, such as membranes, in a directed fashion. Our approach of integrating a minimal model with physical measurements provides insight into general cell-wall regulatory mechanisms that may also be applicable to many walled organisms beyond Gram-positive bacteria.

SUPPORTING MATERIAL

Supporting analysis and six figures are available at http://www.biophysj.org/biophysj/supplemental/S0006-3495(13)00515-8.

The authors thank David Halladin and Tristan Ursell for guidance with EM analysis, Kumaran Ramamurthi for the FC332 and AH93 strains, and Ned Wingreen and members of the Huang laboratory for useful discussions.

This work was funded in part by National Science Foundation (NSF) grant EF-1038697 to A.G., a James S. McDonnell Foundation Award to A.G., an NSF CAREER Award MCB-1149328 to K.C.H., and the Simbios NIH Center for Biomedical Computation at Stanford under grant U54 GM072970 (E.R.R. and K.C.H.).

REFERENCES

1. Whatmore, A. M., and R. H. Reed. 1990. Determination of turgor pressure in *Bacillus subtilis*: a possible role for K+ in turgor regulation. *J. Gen. Microbiol.* 136:2521–2526.
2. Minc, N., A. Boudaoud, and F. Chang. 2009. Mechanical forces of fission yeast growth. *Curr. Biol.* 19:1096–1101.
3. Rojas, E. R., S. Hotton, and J. Dumais. 2011. Chemically mediated mechanical expansion of the pollen tube cell wall. *Biophys. J.* 101:1844–1853.

4. Katifori, E., S. Alben, …, J. Dumais. 2010. Foldable structures and the natural design of pollen grains. *Proc. Natl. Acad. Sci. USA.* 107:7635–7639.
5. Young, K. D. 2006. The selective value of bacterial shape. *Microbiol. Mol. Biol. Rev.* 70:660–703.
6. Scheffers, D.-J., and M. G. Pinho. 2005. Bacterial cell wall synthesis: new insights from localization studies. *Microbiol. Mol. Biol. Rev.* 69:585–607.
7. Koch, A. 1986. The growth strategy of the Gram-positive rod. *FEMS Microbiol. Lett.* 32:247–254.
8. Huang, K. C., R. Mukhopadhyay, …, N. S. Wingreen. 2008. Cell shape and cell-wall organization in Gram-negative bacteria. *Proc. Natl. Acad. Sci. USA.* 105:19282–19287.
9. Furchtgott, L., N. S. Wingreen, and K. C. Huang. 2011. Mechanisms for maintaining cell shape in rod-shaped Gram-negative bacteria. *Mol. Microbiol.* 81:340–353.
10. Boulbitch, A., B. Quinn, and D. Pink. 2000. Elasticity of the rod-shaped gram-negative eubacteria. *Phys. Rev. Lett.* 85:5246–5249.
11. van Teeffelen, S., S. Wang, …, Z. Gitai. 2011. The bacterial actin MreB rotates, and rotation depends on cell-wall assembly. *Proc. Natl. Acad. Sci. USA.* 108:15822–15827.
12. Wang, S., L. Furchtgott, …, J. W. Shaevitz. 2012. Helical insertion of peptidoglycan produces chiral ordering of the bacterial cell wall. *Proc. Natl. Acad. Sci. USA.* 109:E595–E604.
13. Pink, D., J. Moeller, …, T. Beveridge. 2000. On the architecture of the gram-negative bacterial murein sacculus. *J. Bacteriol.* 182:5925–5930.
14. Yao, X., M. Jericho, …, T. Beveridge. 1999. Thickness and elasticity of gram-negative murein sacculi measured by atomic force microscopy. *J. Bacteriol.* 181:6865–6875.
15. Deng, Y., M. Sun, and J. W. Shaevitz. 2011. Direct measurement of cell wall stress stiffening and turgor pressure in live bacterial cells. *Phys. Rev. Lett.* 107:158101.
16. Firtel, M., G. Henderson, and I. Sokolov. 2004. Nanosurgery: observation of peptidoglycan strands in *Lactobacillus helveticus* cell walls. *Ultramicroscopy.* 101:105–109.
17. Touhami, A., M. H. Jericho, and T. J. Beveridge. 2004. Atomic force microscopy of cell growth and division in *Staphylococcus aureus*. *J. Bacteriol.* 186:3286–3295.
18. Tuson, H. H., G. K. Auer, …, D. B. Weibel. 2012. Measuring the stiffness of bacterial cells from growth rates in hydrogels of tunable elasticity. *Mol. Microbiol.* 84:874–891.
19. Koch, A. L. 1983. The surface stress theory of microbial morphogenesis. *Adv. Microb. Physiol.* 24:301–366.
20. Koch, A. L., and R. J. Doyle. 1985. Inside-to-outside growth and turnover of the wall of gram-positive rods. *J. Theor. Biol.* 117:137–157.
21. Matias, V. R. F., and T. J. Beveridge. 2005. Cryo-electron microscopy reveals native polymeric cell wall structure in *Bacillus subtilis* 168 and the existence of a periplasmic space. *Mol. Microbiol.* 56:240–251.
22. Fan, D. P., and M. M. Beckman. 1971. Mutant of *Bacillus subtilis* demonstrating the requirement of lysis for growth. *J. Bacteriol.* 105:629–636.
23. Mauck, J., L. Chan, and L. Glaser. 1971. Turnover of the cell wall of Gram-positive bacteria. *J. Biol. Chem.* 246:1820–1827.
24. Boothby, D., L. Daneo-Moore, …, G. D. Shockman. 1973. Turnover of bacterial cell wall peptidoglycans. *J. Biol. Chem.* 248:2161–2169.
25. Illing, N., and J. Errington. 1991. The *spoIIIA* operon of *Bacillus subtilis* defines a new temporal class of mother-cell-specific sporulation genes under the control of the σ E form of RNA polymerase. *Mol. Microbiol.* 5:1927–1940.
26. Higgins, M. L., J. Coyette, and G. D. Shockman. 1973. Sites of cellular autolysis in *Lactobacillus acidophilus*. *J. Bacteriol.* 116:1375–1382.
27. Meyer, P., J. Gutierrez, …, J. Dworkin. 2010. Cell wall synthesis is necessary for membrane dynamics during sporulation of *Bacillus subtilis*. *Mol. Microbiol.* 76:956–970.
28. Gutierrez, J., R. Smith, and K. Pogliano. 2010. SpoIID-mediated peptidoglycan degradation is required throughout engulfment during *Bacillus subtilis* sporulation. *J. Bacteriol.* 192:3174–3186.
29. Kierzkowski, D., N. Nakayama, …, R. S. Smith. 2012. Elastic domains regulate growth and organogenesis in the plant shoot apical meristem. *Science.* 335:1096–1099.
30. Sliusarenko, O., J. Heinritz, …, C. Jacobs-Wagner. 2011. High-throughput, subpixel precision analysis of bacterial morphogenesis and intracellular spatio-temporal dynamics. *Mol. Microbiol.* 80:612–627.
31. Thwaites, J. J., and N. H. Mendelson. 1989. Mechanical properties of peptidoglycan as determined from bacterial thread. *Int. J. Biol. Macromol.* 11:201–206.
32. Pilizota, T., and J. W. Shaevitz. 2012. Fast, multiphase volume adaptation to hyperosmotic shock by *Escherichia coli*. *PLoS ONE.* 7:e35205.
33. Cayley, D. S., H. J. Guttman, and M. T. Record, Jr. 2000. Biophysical characterization of changes in amounts and activity of *Escherichia coli* cell and compartment water and turgor pressure in response to osmotic stress. *Biophys. J.* 78:1748–1764.
34. Gan, L., S. Chen, and G. J. Jensen. 2008. Molecular organization of Gram-negative peptidoglycan. *Proc. Natl. Acad. Sci. USA.* 105:18953–18957.
35. Hayhurst, E. J., L. Kailas, …, S. J. Foster. 2008. Cell wall peptidoglycan architecture in *Bacillus subtilis*. *Proc. Natl. Acad. Sci. USA.* 105:14603–14608.
36. Koch, A. L. 2002. Why are rod-shaped bacteria rod shaped? *Trends Microbiol.* 10:452–455.
37. Mendelson, N. H., J. E. Sarlls, …, R. E. Goldstein. 2000. Chiral self-propulsion of growing bacterial macrofibers on a solid surface. *Phys. Rev. Lett.* 84:1627–1630.
38. Koschwanez, J. H., K. R. Foster, and A. W. Murray. 2011. Sucrose utilization in budding yeast as a model for the origin of undifferentiated multicellularity. *PLoS Biol.* 9:e1001122 (Erratum in *PLoS Biol*. 2011. 9:10.1371).
39. Fan, D. P., M. C. Pelvit, and W. P. Cunningham. 1972. Structural difference between walls from ends and sides of the rod-shaped bacterium Bacillus subtilis. *J. Bacteriol.* 109:1266–1272.
40. Dyson, R. J., L. R. Band, and O. E. Jensen. 2012. A model of crosslink kinetics in the expanding plant cell wall: yield stress and enzyme action. *J. Theor. Biol.* 307:125–136.
41. Garner, E. C., R. Bernard, …, T. Mitchison. 2011. Coupled, circumferential motions of the cell wall synthesis machinery and MreB filaments in *B. subtilis*. *Science.* 333:222–225.
42. Domínguez-Escobar, J., A. Chastanet, …, R. Carballido-López. 2011. Processive movement of MreB-associated cell wall biosynthetic complexes in bacteria. *Science.* 333:225–228.
43. Zhou, X., and L. Cegelski. 2012. Nutrient-dependent structural changes in *S. aureus* peptidoglycan revealed by solid-state NMR spectroscopy. *Biochemistry.* 51:8143–8153.